Optimized NUFFTs for Interpolations in Back-Projection Algorithms

Amedeo Capozzoli, Claudio Curcio, and Angelo Liseno

Abstract – We deal with the interpolation problem of the back-projection (BP), fast BP (FBP), and fast factorized BP (FFBP) algorithms used in synthetic-aperture radar. The needed 1D and 2D interpolations must be properly performed to achieve accurate results and can be effectively worked out by adopting 1D and 2D nonuniform fast Fourier transform (NUFFT) routines. We generalize a recently developed optimized 1D NUFFT approach to 2D and show the performance improvement when adopted in BP, FBP, and FFBP.

1. Introduction

Synthetic-aperture radar (SAR) back-projection (BP) is widely considered as an appealing approach for high-resolution SAR [1, 2]. It offers many advantages over traditional SAR processing, such as undistorted wave front curvature, accommodating digital topographical elevation maps and ultra-wideband and/or near-field data, and inherently performing motion compensation [3]. BP costs at least $\mathcal{O}(N^3)$ for an $N \times N$ image and needs acceleration to be practical. To this end, the fast BP (FBP) [4] and fast factorized BP (FFBP) [5, 6], reducing the cost to $\mathcal{O}(N^{5/2})$ and $\mathcal{O}(N^2 \log N)$, respectively, have been devised.

FBP and FFBP trade off accuracy and complexity. Their accuracy is dictated in part by the subaperture partitioning and the estimate of the angular sampling step and in part by the interpolation error. While in BP the image is directly evaluated in the final computational grid, in FBP interpolations are needed to regrid partial images to the final lattice, and in FFBP the interpolation process is more in-rolled. Interpolation errors can then accumulate, and the best results can be obtained by a joint use of an optimal sampling and an optimal interpolation. Obviously, by using oversamplings, less accurate interpolation schemes are adoptable. In [4], a 1.3% error is achieved and deemed acceptable by exploiting linear interpolation and an oversampling of 4. Nevertheless, by employing better interpolations, a comparable or an even better accuracy can be reached by coarser samplings.

We have shown that the computations of BP [7] and of the partial images in FBP and FFBP [8] can be conveniently performed by 1D nonuniform fast Fourier transforms (NUFFTs) [9] and that the 2D interpolations in FBP and FFBP can be accurately and quickly calculated, namely, with reduced computational cost, by 2D NUFFTs. Indeed, 1D and 2D NUFFTs achieve a $\mathcal{O}(N \log N)$ and $\mathcal{O}(N^2 \log N)$ complexity, respectively. Furthermore, the NUFFT parameters can be modulated according to the requested accuracy and to the use of single/double precision so that both reach a very convenient trade-off between complexity and accuracy. Finally, 2D NUFFTs are particularly suited for the interpolation of band-limited functions, as those involved in FBP and FFBP, when weak information on the signal band limitedness is available.

NUFFTs achieve high accuracy and the same complexity of standard FFTs thanks to the choice of the interpolation window used to express "nonuniformly" sampled exponentials by "uniformly" sampled ones. In [10, 11], we have presented an optimized approach for NUFFT algorithms based on a general and new perspective. The window has been optimized to obtain more accurate results than those available in the literature without burdening the computational and memory requirements. However, the approach in [10, 11] has been limited to 1D.

The purpose of this article [12] is to present an improvement over the approaches in [2, 7, 8] that dealt with BP, FBP, and FFBP using NUFFT algorithms based on the use of Kaiser–Bessel (KB) windows. In particular, here we use "optimized" NUFFTs developed according to the scheme in [10, 11] for BP, FBP, and FFBP. We show that the use of optimized NUFFTs improves accuracy of about one order of magnitude as compared to the KB case.

In this article, the performance is intentionally evaluated in terms of the number of required operations and of accuracy but not of computation time. Indeed, the time taken by actual implementations strongly depends on, besides the computational complexity of the algorithm, software/hardware factors, such as memory latencies or exploitation of cache memories and pipelines, which are here beyond our scope. As an example, a sequential algorithm with reduced complexity can require larger computing times than a simpler algorithm with larger complexity but amenable to a parallelization profiting of multicore architectures.

2. NUFFT-Based BP

The SAR geometry is illustrated in Figure 1. For the sake of simplicity, a rectilinear trajectory is considered just to illustrate the approach, but the numerical examples will refer to curved paths. Furthermore, the scenario is assumed to be flat.

Here, we use the following symbols: t, slow time; c, light speed; $\underline{r}_a(t) = (x_a(t), y_a(t), z_a(t))$, flight trajec-

Manuscript received 26 August 2020.

Amedeo Capozzoli, Claudio Curcio, and Angelo Liseno are with Universitá di Napoli Federico II, DIETI, via Claudio 21, I 80125 Naples, Italy; e-mail: a.capozzoli@unina.it.

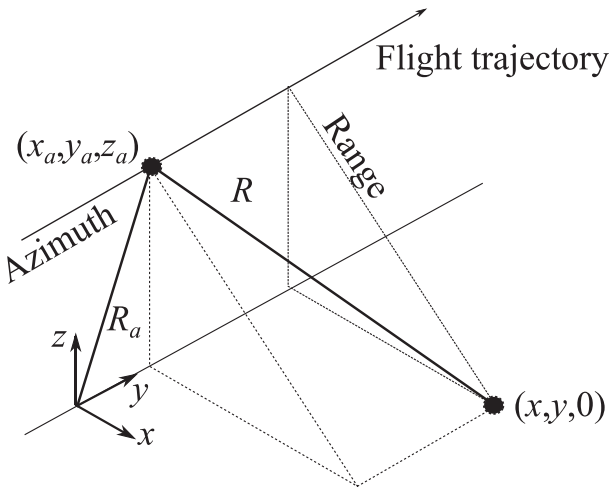

Figure 1. The considered SAR geometry.

tory; and (x, y), ground coordinates. The $z = 0$ plane is the imaging plane.

BP approximates the ground reflectivity $\gamma(x, y)$ by the quantity $h(x, y)$ as [2]

$$h(x,y) = \sum_n \int S(t_n,f) e^{j2\pi f \frac{2\Delta R(x,y,t_n)}{c}} df, \qquad (1)$$

where t_n is the slow-time instant at which the nth pulse illuminating the scene is sent, $S(t_n,f)$ is the nth frequency domain signal after range compression, f is the frequency, $\Delta R(x,y,t_n) = R(x,y,t_n) - R_a(t_n)$, $R_a(t_n) = ||\underline{r}_a(t_n)||$ is the distance between the origin and the platform, $R(x,y,t_n) = ||\underline{r} - \underline{r}_a(t_n)||$ is the distance between the platform and a generic scatterer located at $\underline{r}$, and $\underline{r} = (x,y,0)$ is the position of the generic scatterer.

Let us suppose the image grid to be the Cartesian grid (x_i, y_k). (1) then becomes

$$h(x_i,y_k) = \sum_n \sum_q S(t_n,f_q) e^{j2\pi f_q \frac{2\Delta R((x_i,y_k),t_n)}{c}} \Delta f. \qquad (2)$$

The expression of a 1D nonuniform discrete Fourier transform (NUDFT) of nonequispaced results (NER) type between $\{z_q\}_{q=-Q/2}^{q=Q/2-1}$ and $\{\hat{z}_p\}_{p=1}^{P}$ is the following [11]:

$$\hat{z}_p = \sum_{q=-Q/2}^{Q/2-1} z_q e^{-j2\pi \frac{q}{Q} x_p}, \qquad (3)$$

where the sampling locations x_p must belong to $[-P/2, P/2]$.

Accordingly, the internal summation in (2) is a 1D-NER NUDFT and thus can be efficiently and effectively computed by using a 1D-NER NUFFT [8, 11], the input sampling f_q being regular but the output sampling defined by $2\Delta R((x_i,y_k),t_n)/c$ being irregular.

3. FBP and NUFFT-Based Interpolations

FBP divides the aperture into smaller subapertures of length l (Figure 2), each associated to a partial image $h_m(x, y)$ [4]. The final image is obtained as a coherent superposition of the $h_m(x, y)$'s, namely,

$$\begin{aligned} h(x,y) &= \sum_m h_m(x,y) \\ &= \sum_m \sum_n s\left(t_{mn}, \frac{2\Delta R((x,y),t_{mn})}{c}\right), \end{aligned} \qquad (4)$$

where t_{mn} is the generic sampling point of the mth subaperture and $s(t_{mn}, \tau)$ is the inverse Fourier transform of $S(t_{mn}, f)$. Each $h_m(x, y)$ can be efficiently and effectively computed according to the above BP scheme and, thus, by a 1D-NER NUFFT.

The partial images can be computed in a faster way than BP with a controllable accuracy. Indeed, the sampling requirements for FBP are relaxed as compared to BP. To briefly recall this point, we let $\bar{t}_m$ be the slow time at the center of the mth subaperture so that the generic sampling point t_{mn} of the mth subaperture can be rewritten by aid of the center offsets ξ_n as $t_{mn} = \xi_n + \bar{t}_m$. We also introduce a polar coordinate system $(\rho_m(x,y), \alpha_m(x,y))$ for the mth subaperture defined as (Figure 2)

$$\begin{cases} \rho_m = |\underline{r} - \underline{r}_a(\bar{t}_m)| \\ \cos\alpha_m = \frac{(\underline{r} - \underline{r}_a(\bar{t}_m)) \cdot (\underline{r}_a(\xi_n + \bar{t}_m) - \underline{r}_a(\bar{t}_m))}{\rho_m \xi_n} \end{cases} \qquad (5)$$

with $\underline{r} = (x,y,0)$. Since

$$\begin{aligned} &\Delta R(x,y,\xi_n + \bar{t}_m) \\ &= \sqrt{\rho_m^2(x,y) + \xi_n^2 - 2\rho_m(x,y)\xi_n \cos\alpha_m(x,y)} \\ &\quad - R_a(\xi_n + \bar{t}_m), \end{aligned} \qquad (6)$$

the partial images can be regarded as a function of the polar coordinate systems, that is, $h_m = h_m(\rho_m, \alpha_m)$. A uniform "polar" grid (ρ_{mh}, α_{mr}) can be chosen according to the following steps [4]:

$$\Delta\rho_m \le \frac{c}{2BW}, \quad \Delta(\cos\alpha_m) \le \frac{c}{2f_b l}, \qquad (7)$$

where BW and f_b are the bandwidth and the maximum pulse frequency, respectively, and c is the free-space propagation speed. The angular resolution is inversely proportional to l, which means that keeping l small enables weakening the angular sampling requirements.

The partial images h_m are computed on an uniform polar grid instead of a uniform Cartesian one. Since the polar coordinates (ρ_m, α_m) change from partial image to partial image, FBP requires a final 2D polar-to-Cartesian interpolation onto the common Cartesian grid $(i\Delta x, k\Delta y)$. Such interpolation must be computationally convenient and accurate to avoid the error accumulation [4].

Note that the uniform Cartesian grid $(i\Delta x, k\Delta y)$ appears as a nonuniform grid in polar coordinates, so we must interpolate from a uniform spatial grid to a

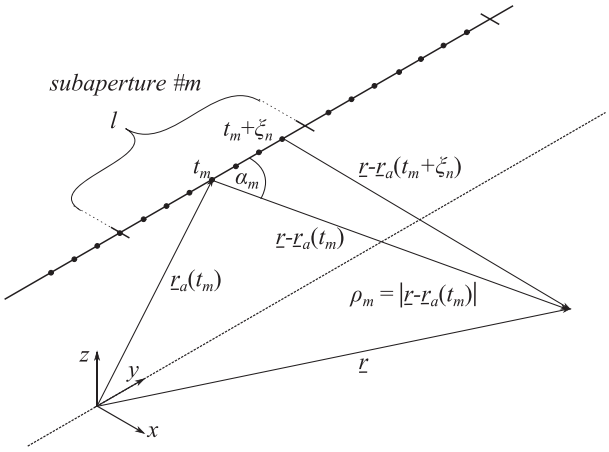

Figure 2. Relevant geometry for the FBP algorithm.

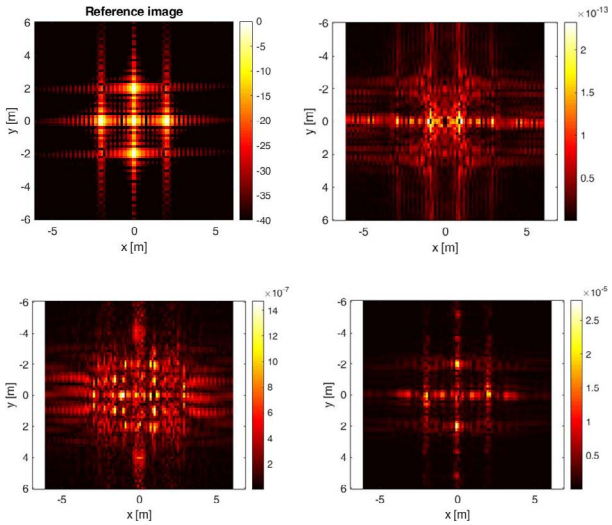

Figure 3. Top left: reference image obtained by BP using a 1D NUDFT in decibel scale. Top right: error for the BP approach. Bottom left: error for the FBP approach. Bottom right: error for the FFBP approach.

nonuniform spatial one. To define the interpolation scheme, it exploits weak information on the band limitedness of the involved functions and is, for Cartesian uniform grids, performed by FFT, zero padding, and inverse FFT. For the specific case of FBP and FFBP, the output is needed over a nonuniform, non-Cartesian grid. Accordingly, NER-NUFFT replaces the inverse FFT stage. As mentioned, the error of FBP is the cumulative effect of both sampling and interpolation errors. A reduction of the total error is expected if the performance of the interpolation stage is improved. For example, since in [4] linear interpolation is adopted and since NUFFT interpolation outperforms the linear one [8], a sensitive reduction of the overall error could be achieved even for nonoptimized NUFFTs and for reduced angular oversampling factors.

While in [8] we employed a NUFFT algorithm for FBP based on the use of KB windows, here we will present an FBP approach using a NUFFT exploiting the optimized one developed in [10, 11].

4. FFBP and 2D NUFFT-Based Interpolations

FFBP uses a tree-based scheme reiterating FBP and in which the interpolation errors can accumulate. It recursively subdivides the subapertures into sub-sub-apertures. Subapertures of level $b-1$ are subdivided into subapertures of level b. The set of subapertures of any level is organized in a tree-like structure.

The calculation of partial images associated to the lowest-level subapertures can be obtained by a BP scheme on a polar grid. Since each subaperture is associated to its own polar grid, climbing up the tree requires a 2D polar-to-polar interpolation [5] since a uniform grid at level b appears nonuniform at level $b-1$ [8]. At the last stage of the tree climbing, FFBP requires, just as FBP, a final 2D polar-to-Cartesian interpolation.

The polar-to-polar interpolation can be performed by a two-step procedure using a standard FFT and a 2D-NER NUFFT [8]. Finally, the polar-to-Cartesian interpolation can be performed as for FBP.

As for FBP, in [8] we employed a KB-NUFFT for FFBP, while here we will present an FFBP scheme using optimized NUFFTs based on the approach in [10, 11].

5. Numerical Results

We present an analysis to show the performance of the optimized NUFFT in BP, FBP, and FFBP.

To this end, we have considered a 12 m × 12 m scene with five point scatterers located at (0, 0) m, (2, 0) m, (–2, 0) m, (0, 2) m, and (0, –2) m. Flight height and depression angle are 7 km and $\pi/4$, respectively, while the number of pulses (azimuth positions) is 1024. Center frequency and bandwidth are 9.6 GHz and 800 MHz, respectively. A curvilinear trajectory with

$$\begin{cases} x(\sigma) = R_0 \cos(\theta_d)(1 + 0.002 * \sin(2\pi\sigma/L)) \\ y(\sigma) = \sigma \\ z(\sigma) = R_0 \sin(\theta_d)(1 + 0.003 * \sin(2\pi\sigma/L)) \end{cases} \quad (8)$$

has been considered, where σ is the representation parameter and L is the length of the synthetic aperture.

We assess BP, FBP, and FFBP using optimized NUFFTs against the reference image obtained by the BP approach using 1D nonuniform discrete Fourier transforms (NUDFTs) [11] shown on the top left of Figure 3. The reconstruction errors obtained by the BP,

Table 1. RMS values for the different interpolation algorithms

Algorithm	KB (%)	Optimized (%)
BP	4.16×10^{-10}	4.79×10^{-11}
FBP	1.8×10^{-3}	3.4×10^{-4}
FFBP	2.6×10^{-3}	6.1×10^{-4}

Table 2. Accuracy of FBP and FFBP with KB-based and optimized NUFFTs. The first column denotes the approach. The subsequent columns represent the number of pulses per subaperture. The accuracy is expressed in terms of percentage RMS errors against the NUDFT-based corresponding schemes

	Pulses							
Approach	4	8	16	32	64	128	256	512
FBP/KB (%)	1.9×10^{-3}	1.8×10^{-3}	1.9×10^{-3}	1.8×10^{-3}	1.8×10^{-3}	1.9×10^{-3}	1.8×10^{-3}	1.9×10^{-3}
FBP/Opt (%)	3.8×10^{-4}	3.7×10^{-4}	3.9×10^{-4}	3.4×10^{-4}	3.6×10^{-4}	3.7×10^{-4}	3.7×10^{-4}	3.9×10^{-4}
FFBP/KB (%)	8.4×10^{-2}	3.1×10^{-3}	2.9×10^{-3}	2.6×10^{-3}	2.2×10^{-3}	1.9×10^{-3}	1.9×10^{-3}	1.7×10^{-3}
FFBP/Opt (%)	8.8×10^{-4}	7.4×10^{-4}	6.7×10^{-4}	6.1×10^{-4}	5.6×10^{-4}	4.7×10^{-4}	3.6×10^{-4}	2.7×10^{-4}

FBP, and FFBP are shown on the top right, bottom left, and right of Figure 3, respectively. FBP and FFBP have been run with (minimum size for FFBP) subapertures of 32 pulses and an angular sampling $\Delta\alpha_m$ with an oversampling of 3. The oversampling of $\Delta\alpha_m$ will be discussed shortly.

The performance of optimized NUFFT can be modulated according to the window enabling the trade-off between accuracy and burden [11]. Single-precision and double-precision modalities can be defined [11]. This fits well the modulation of the trade-off between accuracy and computational burden while moving from BP to FBP and FFBP. Therefore, BP has been run with double-precision NUFFTs. With FBP and FFBP being appointed to renounce to accuracy in favor of computational lightness, for them, single-precision NUFFTs have been run. Single precision is interesting to perform on-the-fly processings on onboard platforms [13] or when acceleration is achieved by GPUs [2] or field-programmable gate arrays (FPGAs) [13] and memory saving is important. Table 1 summarizes the percentage root-mean-square (RMS) errors committed by BP, FBP, and FFBP against the NUDFT-based, reference BP approach. The NUFFT performance critically depends on the interpolation window, and the optimized NUFFTs have better performance when compared to other literature approaches. Table 2 points out the modularity of the optimized NUFFTs and that they outperform other literature approaches. The comparison is performed against the KB window [9], which, in turn, outperforms several competing approaches [11]. The performance is examined with reference also to (minimum size for FFBP) subapertures with different numbers of pulses. Dealing with a better-performing interpolator, as before, the angular sampling step in (7) has been considered with an oversampling of 3, which is reduced against the oversampling of 4 considered in [4]. Notwithstanding the reduced angular oversampling, a percentage error of $\simeq 10^{-4}$ is reached by the optimized single-precision NUFFTs, which is far better than the 1.3% error in [4]. This suggests that FFBP is not far from FBP and confirms that improvements can be achieved in FBP when highly performing interpolators are employed. It is stressed that the optimized NUFFTs are capable of outperforming the KB NUFFTs, gaining an accuracy of almost one order of magnitude.

6. Conclusions

We have proposed BP, FBP, and FFBP based on 1D and 2D optimized NUFFTs. The modularity of NUFFT and BP approaches to trade off accuracy and computational burden has been shown. The better performance of the optimized NUFFTs against KB has been pointed out. We have shown that even when reducing the angular oversampling, performance with accuracy improved by orders of magnitude has been achieved. The NUFFTs based on the KB and optimized windows have the same asymptotic computational complexity (number of operations and memory storage) [10, 11]. However, our optimized window reaches a higher accuracy thanks to its specific design for the NUFFT computation. This is a typical trade-off of accuracy versus computational complexity. Once the input/output nonuniform grid has been defined, the values of the optimized window can be stored and "recycled" for different runs.

Although in BP double-precision accuracy can be of interest when demanded by the application, implementing FBP and FFBP using a single-precision modality can be convenient according to the adopted sampling rate. Examples of that are onboard processing or the case in which the computations are accelerated by GPUs or FPGAs and saving memory space is necessary.

7. References

1. L. A. Horham and L. J. Moore, "SAR Image Formation Toolbox for MATLAB," *Proceedings of SPIE 7699, Algorithms for Synthetic Aperture Radar Imagery XVII*, **769906**, April 2010, doi:10.1117/12.855375.
2. A. Capozzoli, C. Curcio, A. Di Vico, and A. Liseno, "NUFFT- & GPU-Based Fast Imaging of Vegetation," *IEICE Transactions on Communications*, **E94.B**, 7, July 2011, pp. 2092-2103.
3. M. Rodriguez-Cassola, P. Prats, G. Krieger, and A. Moreira, "Efficient Time-Domain Image Formation With Precise Topography Accommodation for General Bistatic SAR Configurations," *IEEE Transactions on Aerospace Electronic Systems*, **47**, 4, October 2011, pp. 2949-2966.
4. A. F. Yegulalp, "Fast Backprojection Algorithm for Synthetic Aperture Radar," IEEE Radar Conference, Waltham, MA, USA, April 20–22, 1999, pp. 60-65.
5. L. M. H. Ulander, H. Hellsten, and G. Stenström, "Synthetic Aperture Radar Processing Using Fast Factorized Back-Projection," *IEEE Transactions on Aerospace Electronic Systems*, **39**, 3, July 2003, pp. 760-776.
6. P. O. Frölind and L. M. H. Ulander, "Evaluation of Angular Interpolation Kernels in Fast Back-Projection

SAR Processing," *IEE Proceedings—Radar, Sonar and Navigation*, **153**, 3, June 2006, pp. 243-249.
7. A. Capozzoli, C. Curcio, and A. Liseno, "Fast GPU-Based Interpolation for SAR Backprojection," *Progress in Electromagnetics Research*, **133**, January 2013, 259-283.
8. A. Breglia, A. Capozzoli, C. Curcio, and A. Liseno, "NUFFT-Based Interpolation in Backprojection Algorithms," *IEEE Geoscience and Remote Sensing Letters*, in press, doi:10.1109/LGRS.2020.3013444.
9. K. Fourmont, "Non-Equispaced Fast Fourier Transforms With Applications to Tomography," *Journal of Fourier Analysis and Applications*, **9**, 5, September 2003, pp. 431-450.
10. A. Capozzoli, C. Curcio, and A. Liseno, "An Approach to NUFFT Optimization," XXII Riunione Nazionale di Elettromagnetismo, Cagliari, Italy, September 3–6, 2018, 4 pp.
11. A. Capozzoli, C. Curcio, and A. Liseno, "Optimized Non-Uniform FFTs (NUFFTs) and Their Application to Array Factor Computation," *IEEE Transactions on Antennas and Propagation*, **67**, 6, June 2019, pp. 3924-3938.
12. A. Capozzoli, C. Curcio, and A. Liseno, "Using NUFFTs for Interpolations of Fast Backprojection Algorithms," URSI 2020 General Assembly and Scientific Symposium, Rome, Italy, August 29–September 5, 2020, pp. 1-3.
13. W. Li, Z. Xu, and D. Zhu, "The FPGA Implementation of Real-Time Spotlight SAR Imaging," International Geoscience and Remote Sensing Symposium, Valencia, Spain, July 22–27, 2018, pp. 6703-6706.